Chemical Composition of Diesel/Biodiesel Particulate Exhaust by FTIR Spectroscopy and Mass Spectrometry: Impact of Fuel and Driving Cycle

Olga B. Popovicheva, Cornelia Irimiea, Yvain Carpentier, Ismael Ortega, Elena D. Kireeva, Natalia K. Shonija, Jaroslav Schwarz, Michal Vojtíšek-Lom, Cristian Focsa

Aerosol and Air Quality Research, 17: 1717–1734, 2017

ISSN: 1680-8584 print / 2071-1409 online
doi: 10.4209/aaqr.2017.04.0127

Chemical Composition of Diesel/Biodiesel Particulate Exhaust by FTIR Spectroscopy and Mass Spectrometry: Impact of Fuel and Driving Cycle

Olga B. Popovicheva[1*], Cornelia Irimiea[2], Yvain Carpentier[2], Ismael K. Ortega[2,3], Elena D. Kireeva[1], Natalia K. Shonija[4], Jaroslav Schwarz[5], Michal Vojtíšek-Lom[6], Cristian Focsa[2]

[1] *Skobeltsyn Institute of Nuclear Physics, Lomonosov Moscow State University, Moscow, 119991, Russian Federation*
[2] *Univ. Lille, CNRS, UMR 8523 – PhLAM – Physique des Lasers Atomes et Molécules, F-59000 Lille, France*
[3] *Onera – The French Aerospace Lab, F-91761 Palaiseau, France*
[4] *Chemical Department, Lomonosov Moscow State University, Moscow, 119991, Russian Federation*
[5] *Institute of Chemical Process Fundamentals CAS, Prague, CZ-16502, Czech Republic*
[6] *Center for Sustainable Mobility, Czech Technical University in Prague, CZ-16607, Czech Republic*

ABSTRACT

The growing concern about air quality and the impact exhaust particles can have on the environment has resulted in the increased use of alternative fuels. A sampling campaign from a conventional heavy diesel engine operated in typical transient cycle or steady-state condition, and running on diesel, 30% biodiesel in diesel, and 100% biodiesel was carried out. The particulate composition was characterized using Fourier Transform Infrared (FTIR) spectroscopy, Two-step Laser Mass Spectrometry (L2MS), Secondary Ion Mass Spectrometry (SIMS), thermo-optical analysis, and capillary electrophoresis. Elemental carbon is demonstrated to decrease from diesel to 100% biodiesel, in agreement with the evolution of aromatic bands and the MS abundance of C_n^- fragments, while organic carbon exhibits a constant level irrespective of the working regime. Aliphatic, aromatic, carboxyl, carbonyl, hydroxyl functionalities, and nitro compounds are found to depend on the engine-working regime. Mass spectra are mainly characterized by alkyl fragments ($C_nH_{2n+1}^+$), associated to normal and branched alkanes, PAHs and their alkylated derivatives. The addition of biodiesel to diesel changes the particulate composition towards more oxygenated constituents, such as carbonyl groups attributed to methyl ester CH_3O^+ fragments of unburned biodiesel. Fuel-specific fragments have been identified, such as $C_3H_7O^+$ for diesel, and $C_2H_3O_2^+$ and CH_3O^- for biodiesel. Nitrogenized compounds are revealed by -NO_2 functionalities and N-containing fragments. Principal Component Analysis (PCA) was successfully applied to discriminate the engine operating conditions, with a higher variance given by the fuel, thus allowing to better evaluate the environmental impacts of alternative energy source emissions.

Keywords: Diesel engine; Particulate emission; FTIR; Mass spectrometry; Environmental pollution.

INTRODUCTION

Large amounts of air pollutants are produced worldwide by emission from fossil fuel combustion, including transport, which contributes around 20–25% of total anthropogenic emission of carbonaceous particles (Cofala *et al.*, 2007). In Europe, more than 70% of carbonaceous aerosols originate from the transport sector, while diesel-produced aerosols are considered to be dangerous pollutants. The growing concern about their environmental impact and health hazard in urban areas has resulted in the development of modern combustion engines that emit less particulate matter (PM). Concurrently, alternative fuels, such as vegetable oil-based biofuels (referred to as biodiesel), tend to be used in modern combustion engines (Agarwal, 2007; Giakoumis *et al.*, 2012) in an attempt to further lessen soot particles emission and the concentration of unburned hydrocarbons (HC) and carbon monoxide (CO) released in engine exhausts (Dwivedi *et al.*, 2006; Jung *et al.*, 2006; Betha and Balasubramanian, 2011; Shah *et al.*, 2014).

However, much concern has been expressed in regards to the potential health hazard of diesel and biodiesel fuels. In fact, the high number density at which diesel or biodiesel particles are still emitted in urban areas are thought to exacerbate respiratory, cardiovascular, and allergic diseases due to their small respirable size, large surface area, surface

* Corresponding author.
Tel.: +7 495 939 4954; Fax: +7 495 939 0896
E-mail address: polga@mics.msu.su

reactivity, hygroscopicity, and potential toxicity (Bernstein *et al.*, 2004; Turrio-Baldassarri *et al.*, 2004; Müller *et al.*, 2005; Reff *et al.*, 2007; Popovicheva *et al.*, 2008; Russell *et al.*, 2009; Topinka *et al*., 2012; Steiner *et al*., 2013; Popovicheva *et al.*, 2014a). Specifically, the toxicological properties of diesel and biodiesel PM have been studied by Libalova *et al.* (2016) and showed that human lung cells exposed 24 h to such emission expressed deregulated genes, especially those involved in antioxidant defense and cell cycle regulation and proliferation. Slight changes observed in the biological response to the toxic PM were reported to depend on nature of the fuel. Consequently, as the search for engine performance and fuel efficiency is now a common goal that still requires the development of modern engines fueled with diesel alternatives, a thorough investigation of the PM composition emitted in such engine exhaust is of great importance (Vojtisek-Lom *et al.*, 2012a, b).

PM emitted by fossil fuel combustion contains soot agglomerates of 30–50 nm spherical primary particles exhibiting a characteristic chain-like morphology (Chen *et al*., 2005). Graphite-like microcrystallites make up the elemental carbon microstructure of the primary particles (Popovicheva *et al.*, 2003; Vander Wal *et al.*, 2007). In addition, unburned organic components and inorganic contaminations originating from fuel, lube oil, or/and engine wear may condense at the soot surface. Adsorbed chemical contribution from organic carbon or inorganic fly ash greatly increases the PM overall molecular and structural complexity (Kleeman *et al.*, 2000; Sakurai *et al.*, 2003; Toner *et al.*, 2006). In fact, unburned organic components may make up to 90% of PM mass depending on the engine operating conditions (Chow *et al.*, 2007), and generally account for a significant mass fraction (Coury and Dillner, 2009; Guzman-Morales *et al.*, 2014).

In contrast to conventional diesel made from aliphatic and aromatic hydrocarbons, biodiesel is an oxygenated fuel produced by transesterification of oils. It is made of long-chain alkyl esters, and contains no aromatics or sulfur. An advantage of using biofuel is that it reduces PM mass, particle number, and size as compared to diesel fuel (Betha and Balasubramanian, 2011; Chang *et al.*, 2014). Reduction of polycyclic aromatic hydrocarbons (PAHs) (Lin *et al.*, 2017) and elemental carbon (EC) (Na *et al.*, 2015) emissions were concomitantly observed. Many campaigns have been conducted over the past decade regarding the characterization of air quality degradation resulting from biodiesel/biofuel and diesel-fueled engine emissions (Dwivedi *et al.*, 2006; Betha and Balasubramanian, 2011). Concentrations of volatile and soluble organics, which are indicators of toxicity and carcinogenicity, were found to be higher in biodiesel exhaust compared to diesel. Diesel PM contains substantially more PAHs than rapeseed oil PM, while the carcinogenic PAH level is higher for rapeseed oil exhaust (Topinka *et al.*, 2012). Soot generated by oxygenated fuel has the more oxidized surface, which causes the oxidation to proceed much faster compared to soot generated by diesel (Song *et al.*, 2006). Biofuel particles exhibit specific chemical signatures, such as functional groups in carboxylic acids, ketones, esters, and -NO_2, C-N, and -NH groups in nitro compounds. In addition, surface oxidation in biofuel particles is suggested by the presence of polar oxygenated and non-polar aliphatic functionalities (Popovicheva *et al.*, 2015b). Therefore, the addition of biodiesel to fuel blends, such as methyl ester oils, leads to significant increase of carbonyl, PAH, nitro-PAH, and oxy-PAH compounds (Karavalakis *et al.*, 2011). However, particle-bound PAH emissions are also shown to be variable, depending on the biodiesel blends and operating conditions (Prokopowicz *et al.*, 2015).

Studies regarding the influence of diesel engine operating conditions on PM emission have commonly focused on the engine steady-state performance, i.e., when both the engine speed and the fuel consumption remain constant. However, real-world engine operating conditions likely deviate from this ideal situation and is best represented by a transient cycle, where both engine speed and fuel consumption vary. Therefore, experimental investigations of exhaust emissions are to be expanded to transient diesel engine operation cycles (Giakoumis *et al.*, 2012).

Fourier transform infrared (FTIR) spectroscopy is a powerful tool for PM composition analysis (Bladt *et al.*, 2012; Popovicheva *et al.*, 2014b). However, due to the molecular complexity of combustion particles, the identification of classes of chemical compounds associated to the detected functional groups is challenging (Coates, 2000). In fact, because many broad vibration bands overlap in the spectral region of interest, the interpretation of FTIR spectra is difficult. However, mass spectrometry techniques can provide detailed molecular and fragment identifications making it a valuable complementary analytical tool in aid of particles characterization. Different mass spectrometry techniques have been used in the past for diesel and biodiesel exhausts analyses, including Gas Chromatography Mass Spectrometry (GC-MS) (Pedersen *et al.*, 1999; Casal *et al.*, 2014), Secondary Ion Mass Spectrometry (SIMS) (Kirchner *et al.*, 2003), Thermal Desorption Molecular Beam Mass Spectrometry (TDMBMS) (Tobias *et al.*, 2001; Sakurai *et al.*, 2003) and Laser Desorption Mass Spectrometry (LDMS) (Moldanovà *et al.*, 2009; Maricq *et al.*, 2011). Among these mass spectrometry techniques, SIMS stands out because of its high mass resolution, although it suffers from large fragmentation subsequent to ion impact. In contrast, the Two-step Laser Mass Spectrometry (L2MS) performs a soft desorption and ionization of molecular compounds that generates intact parent molecules. Using various ionization schemes, it is further possible to selectively detect different classes of molecules. Aromatic species can then be detected using a resonant two-photon ionization (R2PI) scheme at 266 nm (Bouvier *et al.*, 2007; Faccinetto *et al.*, 2011, 2015; Delhaye *et al.*, 2017), whereas aliphatic species will be preferentially detected using a single-photon ionization (SPI) scheme at 118 nm (10.5 eV) (Öktem *et al.*, 2004; Ferge *et al.*, 2005).

In order to clarify the molecular complexity in aerosols, complementary measurements of their chemical components (bonds, fragments, and ions) are often used (Russell *et al.*, 2009; Gentner *et al.*, 2012). For instance, SIMS and Single Particle Mass Spectrometry (SPMS) coupled to FTIR were used to characterize the surface composition of diesel

particles (Kirchner *et al.*, 2003). The general agreement between chemical bonds and molecular fragments has been demonstrated by quantifying the organic mass for many ambient and laboratory aerosols (Russell *et al*., 2009).

In this study, the effect of conventional and alternative fuels, as well as that of the operating conditions, on the chemical composition of particles emitted by modern on-road heavy-duty diesel engine is examined using both FTIR spectroscopy and mass spectrometry. These analyses are supported by conventional thermo-optical and capillary electrophoresis techniques. Blends of diesel, 30% biodiesel, and 100% biodiesel are tested on a diesel engine operated in either steady-state condition (1500 rpm and 30% load) or World Harmonized Transient Cycle (WHTC) condition. FTIR spectra are collected to identify C-, H-, N-, and O-containing functional groups, while L2MS and SIMS analyses extend the identification of molecular compounds and fragments in aid of bulk results, demonstrating the important environment-related properties and emission reduction characteristics assigned to engine emissions.

EXPERIMENTAL

An Iveco Tector heavy-duty diesel engine was operated in a dynamometer facility at the Czech Technical University Prague as described in a complementary study (Libalova *et al.*, 2016). It ran in either World Harmonized Transient Cycle (WHTC) with a hot start, whereby the engine reached a stabilized operating temperature at the beginning of the test, or in steady-state regime (1500 rpm and 30% load (210 N m)), which roughly represents the average load of heavy vehicles at highway cruise. The engine was operated without any exhaust after treatment. Neat petroleum diesel (B0), 100% biodiesel (rapeseed oil methyl esters) (B100), and a mixture of 30% (by volume) biodiesel in diesel (B30) were used as fuels. B30 belongs to the new European standard, titled DIN EN 16709. Moreover, blends with up to 30% biodiesel usually does not require any modification of the car engine. Diesel fuel was conventional EN 590 with sulfur and ash content of 350 mg kg^{-1} and 0.01 wt%, respectively. Mineral lubricating oil was used, with Ca, Na, S, K, and Zn content in ash 7–15 times higher than that in fuel, as analyzed in Popovicheva *et al.* (2014a). The diluted exhaust was sampled from a full flow dilution tunnel onto 47 mm diameter quartz filters (Tissuquartz, Pall). The high-dilution flow and the controlled temperature provided by this technique were used to avoid the condensation of the volatile species on the surface of particulate matter. The list of fuels, operating conditions, and extracted part of the engine total work (energy) for each sampling case is presented in Table 1.

Measurements of elemental carbon (EC) and organic carbon (OC) on quartz filters were performed using the OC/EC field analyzer from Sunset Inc. (USA) in accordance with the EUSAAR2 protocol (Cavalli *et al*., 2010). The instrument deploys a thermo-optical transmission method where evaporated and oxidized carbonaceous compounds are detected as carbon dioxide using a non-dispersive infrared (NDIR) detector. The split between OC and EC is determined optically using a laser transmission through the filter. The blank correction was done using the average of five blank filters; the uncertainty of blank value is 0.76 μg cm^{-2}. The total carbon (TC) content was calculated as the sum of corrected OC and EC. The limit of detection (LOD) of the instrument is 0.2 μg cm^{-2} for OC and TC, and 0.1 μg cm^{-2} for EC (Bauer *et al*., 2009). The measured values are provided for each operation condition normalized per kWh of engine work.

Water-soluble ion mass concentrations were determined using a capillary electrophoresis (CE) system (Capel-103, Lumex Corp.). Five inorganic anions (SO_4^{2-}, NO_2^-, Cl^-, F^-, and PO_4^{3-}) and cations (Na^+, NH_4^+, K^+, Mg^{2+}, and Ca^{2+}), as well as three organic ions ($HCOO^-$, CH_3COO^-, $(COO^-)_2$), were measured in aqueous extracts with the relative standard deviation of 10%. One-fourth from each filter sample was extracted in 5 mL distillated water by ultrasonic agitation for 45 min, followed by filtration of the extract solutions. A mixture of benzimidazole, tartaric acid, and 18-crown-6 ether was used as an electrolyte in cation measurements. Anions were analyzed in the chromate buffer prepared from chromium oxide (VI), diethanolamine, and cetyltrimethylammonium hydroxide solution. The LOD for ion concentrations was in the range of 0.1–0.5 mg L^{-1}, depending on the ion type. The measured ion mass concentrations were systematically blank corrected.

FTIR spectra of filter samples were acquired using an IRPrestige-21 spectrometer (Shimadzu, Japan) in diffuse reflection mode described in details elsewhere (Popovicheva *et al*., 2015b, 2016). Spectra were recorded in the 450 to 4000 cm^{-1} range with 4 cm^{-1} resolution and 100 accumulated scans. A reference spectrum taken from a blank filter was acquired prior to analyses and was subsequently subtracted in order to remove IR contributions from the filter and avoid large atmospheric variations in sampled particles spectra. To address the possible inhomogeneity of the sample loading, spectra were collected from five different spots on each sample. If four out of five spectra demonstrated the same absorption bands, we considered these bands as being

Table 1. Diesel engine exhaust particulate sampling conditions, engine work, and EC/OC ratio.

Sample name	Fuel	Operating condition	Engine work (Wh)	EC/OC
DB0T	Diesel B0	WHTC	5.1	2.29
DB0S		1500 rpm, 30% load	2.4	1.66
DB30T	Biodiesel B30	WHTC	6.4	1.11
DB30S		1500 rpm, 30% load	2.9	0.71
DB100T	Biodiesel B100	WHTC	6.4	0.56
DB100S		1500 rpm, 30% load	2.9	0.27

representative of the entire sample. IRsolution software was used to subtract pre-scan from post-scan and then to perform the baseline correction. Because blank filters exhibit strong absorption bands in the 500–1400 cm^{-1} spectral range, the baseline correction does not perfectly cancel out blank contribution in this region and therefore may result in a biased interpretation. Consequently, only absorption bands emerging above 1400 cm^{-1} will be discussed from now on.

The identification of absorption bands was carried out using chemical standards and searches against the Shimadzu FTIR database, which is Coates' practical approach (Coates, 2000). Absorbance peak areas of prominent bands are calculated and the relative intensity of a given functionality is inferred from the ratio of its absorbance area to the total absorbance area over the spectrum.

The surface chemical composition was probed by two mass spectrometry techniques: Two-step Laser Mass Spectrometry (L2MS) and Secondary Ion Mass Spectrometry (SIMS). The home-made L2MS apparatus has been described in detail elsewhere (Focsa and Destombes, 2001; Focsa *et al.*, 2003; Mihesan *et al.*, 2004, 2006). Briefly, the collimated (2-mm diameter) beam of a Nd:YAG laser (Continuum Minilite II, 5 ns, 532 nm, 10 Hz) irradiates the surface of the sample, placed in vacuum (about 10^{-8} mbar residual pressure) on a cryogenic stage. Neutral species in the desorption plume are then ionized by an orthogonal delayed UV light source. The used UV light source is either a Nd:YAG laser beam (Continuum Powerlite 8010, 6 ns, 266 nm, 10 Hz) for the Resonant Two-Photon Ionization (R2PI) of most of the aromatic species (Thomson *et al.*, 2007; Mihesan *et al.*, 2008), or a 118 nm (10.5 eV) focused beam of a coherent source generated by four-wave mixing in a Xe-cell (Butcher *et al*., 1999) and enabling Single Photon Ionization (SPI) of most of the condensable species including aliphatic compounds (Desgroux *et al*., 2013). Both desorption and ionization laser intensities are kept close to the threshold (typically several MW cm^{-2}) to avoid fragmentation of analytes. L2MS spectra have been averaged over 500 desorption laser shots while scanning the surface of the sample. For each ionization scheme, two consecutive spectra were recorded per sample. Both ionization techniques are complementary since the 118 nm beam allows the detection of all species with vertical ionization energy lower than 10.5 eV and the 266 nm permits the selective ionization of most of the aromatic species in a resonant two-photon ionization process. The mass resolution for a distinctive peak belonging to one mass spectrum is $m/\Delta m \approx 10^3$ (m/z 178). For comparison between different sample mass spectra, the ion current has been normalized to the signal of the most intense mass peak (base peak). The L2MS setup is configured for the detection of positive ions only. Mass peaks have been assigned based on the ionization scheme selectivity, according to previous results obtained for known standards (Faccinetto *et al.*, 2011, 2015).

SIMS analysis was performed with a commercial Time-of-flight TOF.SIMS^5 instrument (ION-TOF GmbH). The sample surface was probed in static SIMS mode, where a low dose of primary ions is used to lower the molecule fragmentation. A Bi_3^+ pulsed (about 1 ns) ion beam was accelerated at 25 keV and the secondary positively or negatively charged ions were detected by TOF-MS. The primary ion source delivered a pulsed current of 0.3 pA rastered in 25 scans over a 500 × 500 μm^2 area for an acquisition time of 180 s. The mass resolution of the instrument ranges from 1800 to 3000 depending on the sample surface roughness. Four spectra were recorded for each polarity, i.e., eight spectra per sample. SIMS peaks have been assigned based on the mass accuracy and mass resolution used in the current study.

For each type of working regime, MS results can be arranged in four categories consisting of mass spectra obtained with SPI L2MS, R2PI L2MS, and SIMS in positive polarity and negative polarity. For these data, we applied Principal Component Analysis (PCA), which is an orthogonal transformation that projects a set of observations onto linearly uncorrelated variables denoted as principal components, allowing one to highlight similarities and differences within the dataset (Pei *et al.*, 2008). Each mass spectrum has been represented by a set of values corresponding to the integrated area of selected mass peaks, including a number of 26, 33, and 67 confidently identified compounds for SPI L2MS, negative and positive polarity SIMS, respectively. The determined principal components can thus be expressed in terms of these specific compounds. Routines implemented in Origin 2016 (OriginLab, Northampton, MA) have been used.

RESULTS

OC, EC, and Ions in Bulk Composition

Relative OC/EC ratios in particulate emissions depend on the type of fuel processed in the engine because of their different diesel and biodiesel contents (Jedynska *et al.*, 2015). The masses of OC and EC produced per kWh, when diesel, 100% biodiesel, and 30% biodiesel in diesel are supplied to the Iveco Tector engine operated at WHTC or steady-state (1500 rpm, 30% load) condition are shown in Fig. 1(a). OC is similar for both working regimes, ranging from 23 mg kWh^{-1} for diesel B0 steady-state (DB0S) to 33 mg kWh^{-1} for diesel B30 steady-state (DB30S). EC exhibits a significant reduction with the biofuel content increase, from a maximum of 64 mg kWh^{-1} for transient DB0T to 7 mg kWh^{-1} for steady-state DB100S. The EC concentration decreases from transient to steady-state conditions for all fuels. The decrease of EC with the increase of the biofuel content apparently causes the decrease of total carbon emissions (92 mg kWh^{-1} for diesel to 38 mg kWh^{-1} for 100% biodiesel in transient and from 62 to 35 mg kWh^{-1} in steady-state condition). As a result, the EC/OC ratio decreases from 1.66 and 2.29 for DB0S and DB0T, to 0.27 and 0.56 for DB100S and DB100T, respectively (Table 1).

In contrast to OC and EC content, the ion composition is not determined by the fuel content but mainly by mineral lubricating oil, as shown in Popovicheva *et al.* (2014a). The mass of inorganic ions, namely K^+, Na^+, NH_4^+, Ca^{2+}, SO_4^{2-}, NO_2^-, Cl^-, and PO_4^{3-} ions, and that of organic ions, $HCOO^-$ and $(COO^-)_2$, produced in diesel/biodiesel exhaust emissions per kWh at both operating conditions, are shown

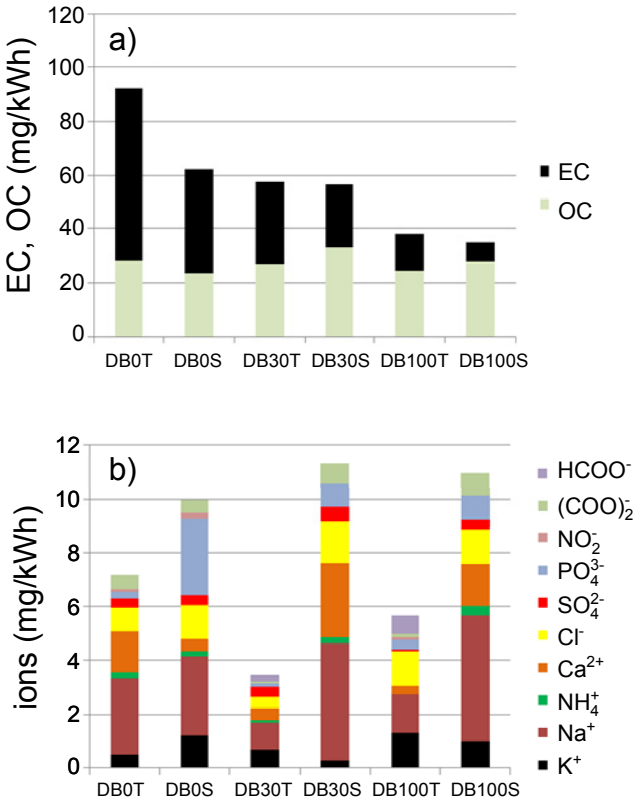

Fig. 1. Mass of a) OC and EC, and b) ions per kWh for diesel/biodiesel runs on the Iveco Tector engine in transient and steady-state conditions.

in Fig. 1(b). The total ion mass does not correlate well with the increase of biodiesel in the fuel. The inorganic ion mass is dominated by Na^+, Ca^{2+}, PO_4^{3-}, and Cl^- for all regimes, similar to that observed in particulate emissions from an Opel Astra diesel engine (Popovicheva *et al.*, 2014a). Concentrations of oxalate $(COO^-)_2$ and formate $HCOO^-$ ions are always lower with respect to the inorganic ones.

IR Absorbance and Functionalities

FTIR spectroscopy measures the absorbance associated with the frequency of the bond and thus reveals the nature of the functional groups representing the various classes of organic compounds in the entire aerosol composition. FTIR studies of the interfaces of diesel and vegetable oil-based biofuel soot showed that they mainly consist of polycyclic aromatic hydrocarbons, nitro and carbonyl functionalities (Tapia *et al.*, 2017). IR spectra of particles emitted from the engine operated in steady-state and transient conditions are shown in Fig. 2. Aliphatic C-C-H and aromatic C=C groups suggest the presence of alkanes and polyaromatic hydrocarbons, respectively. Carboxyl C(O)O and carbonyl C=O groups represent functionalities in carboxylic acids and ketones, esters, anhydrides, quinones, conjugated ketones, respectively. Hydroxyl -OH groups are associated with alcohols and phenols, while aromatic $-NO_2$ and -NH groups indicate the presence of nitrogen-oxy compounds and amines. The absorption peak areas of functional groups are estimated for diesel, 30% biodiesel, and 100% biodiesel fuels. Fig. 3 shows the relative intensities of aliphatic C-C-H, O-containing groups, and aromatic C=C groups in the 2800–3000, 1640–1780, and 1520–1620 cm^{-1} ranges for B0, B30, and B100 fuels, respectively.

Steady-State Condition

Aliphatic compounds accompany the process of soot formation in premixed flames and diesel engine exhausts (Cain *et al.*, 2010). The prominent FTIR spectral features of diesel and biodiesel particles emitted at 1500 rpm 30% load are aliphatic C-C-H symmetric/asymmetric stretches (2857–2928 cm^{-1}) and bends (1463 cm^{-1}) of methylene $> CH_2$ groups in alkanes (Fig. 2(a)). Asymmetric stretches and bends of methyl $-CH_3$ groups emerge as shoulders of the stronger $> CH_2$ bands at 2960 and 1440 cm^{-1}, respectively, in the spectra of 30% and 100% biodiesel. Further analyses reveal the increase of the relative intensity of aliphatic C-C-H groups from 25% to 50% for B0 and B100, respectively (Fig. 3(a)).

The band located at 1725 cm^{-1} can be associated with both carboxylic C(O)O and carbonyl C=O groups in carboxylic acids and ketones/aldehydes, respectively. This band is barely visible for diesel particles. It is reasonable that the use of diesel fuel and mineral lubricating oil, which are not oxygenated produce very few oxygen-containing compounds. If present, they could be produced by the oxidation process occurring during combustion in the engine.

Another band corresponding to a C=O group is observed in 30% biodiesel particles at 1750 cm^{-1}. It relates to carbonyls in anhydrides and esters. An intense band at 1721 cm^{-1} indicates carbonyls in 100% biodiesel. A significant impact of the biofuel on particle composition is in good agreement with observation of high abundance of double bond of C=O in various biofuels (Abdullah *et al.*, 2016) as well as of oxygenated functionalities in rapeseed and palm oil particles emitted by an Opel Astra diesel engine (Popovicheva *et al.*, 2014a) and off-road diesel engines operated in steady-state conditions (Popovicheva *et al.*, 2015b).

A broad band emerging at 1664–1671 cm^{-1} in diesel/biodiesel particles may result from the overlap of unsaturated alkenyl AlC=C (1620–1680 cm^{-1}) and carbonyl C=O vibrations at higher frequencies (1675–1690 cm^{-1}). The same band was identified in the spectra from off-road engines operated in various steady-state conditions, randomly for diesel and almost always for biodiesel particles (Popovicheva *et al.*, 2015a). The stretching of carbonyls with more conjugation than aldehydes, ketones, and acids (e.g., in quinones, conjugated ketones) produces an absorbance in this region. The total relative intensity of oxygenated groups is estimated to be around 5% for B0 and increases up to 15% for B100 (Fig. 3(a)).

The second prominent FTIR spectral feature of diesel and biodiesel particles in any operating conditions is a broad intense band in the range 1570–1620 cm^{-1}, which is the most complicated to assign. It can be attributed to a C=C stretching either in aromatic compounds (Fanning *et al.*, 1993) or in soot particles due to the polyaromatic character of its microcrystalline structure (Akthter *et al.*, 1985). In both cases, the IR-inactive C=C mode is activated by either sufficient asymmetry of the carbon material

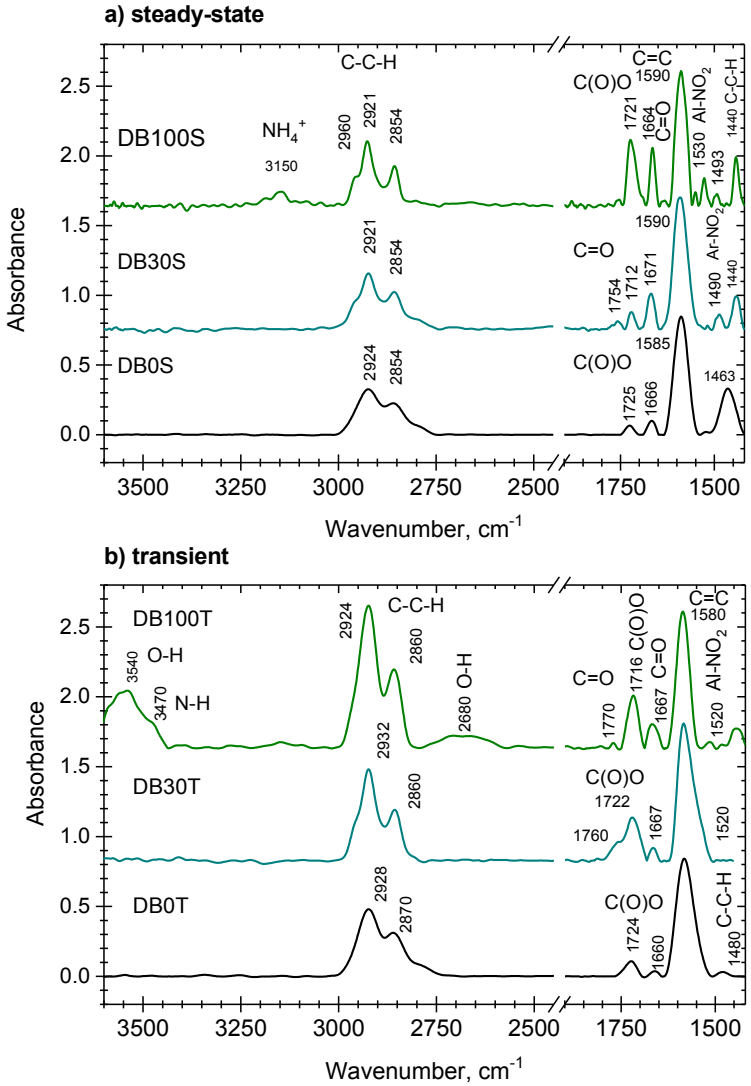

Fig. 2. FTIR spectra of particles emitted by the diesel engine operated in a) steady-state and b) transient conditions, using diesel, 30% biodiesel, and 100% biodiesel. Functionalities and peak positions are indicated.

polyaromatic structure (e.g., by defects) or the presence of adsorbed oxygen. Oxygen-containing functionalities described above can support such activation. The relative intensity of C=C groups in the 1570–1620 cm^{-1} region is estimated to be 60% for B0 and gradually decreases, down to 35% for B100 (Fig. 3(a)). Relatively weak C=C bands in diesel spectra in comparison with biodiesel particles are in accordance with the low abundance of oxygen-containing functionalities in diesel-generated particles.

The same band located at 1580 cm^{-1} was observed in FTIR spectra of diesel particles produced by off-road diesel engines (Popovicheva *et al.*, 2016). However, it was not found in Opel (Popovicheva *et al.*, 2014a) and internal combustion engine-emitted diesel and biodiesel particles (Popovicheva *et al.*, 2015a). Such vibrations may not always be related to the polyaromatic structure of soot particles. Also, we should mention that carboxylate RC(O)O vibrations associated with $RCOO^-$ ions in carboxylic acids and their salts are found in the 1580–1650 cm^{-1} spectral range (Popovicheva *et al.*, 2016). They can broaden the 1580 cm^{-1} band on the high frequency side of the spectrum. This assumption is confirmed by a relatively high concentration of carboxylate ions, predominantly in oxalate form, in steady-state conditions (Fig. 1(b)).

Functionalities of nitro compounds are observed in both B30 and B100 spectra, and their relative intensities increase with the amount of biodiesel. The band at 1490 cm^{-1} associated with aliphatic Al-NO_2 vibrations appears in the 30% biodiesel particles, and is accompanied by vibration of aromatic Ar-NO_2 for 100% biodiesel emission. Spectra of B100 in steady-state condition present a band at 3150 cm^{-1}, which is assigned to the vibration of NH_4^+ ions.

Transient Cycle

Saturated aliphatic C-C-H symmetric/asymmetric stretches (2870–2928 cm^{-1}) and bends (1480 cm^{-1}) of methylene $>CH_2$ groups in alkanes are prominent in FTIR spectra of diesel and biodiesel particles emitted in hot WHTC cycle (Fig. 2(b)). The methyl -CH_3 groups are observed only for B30. Comparative analyses reveal the relative intensity of

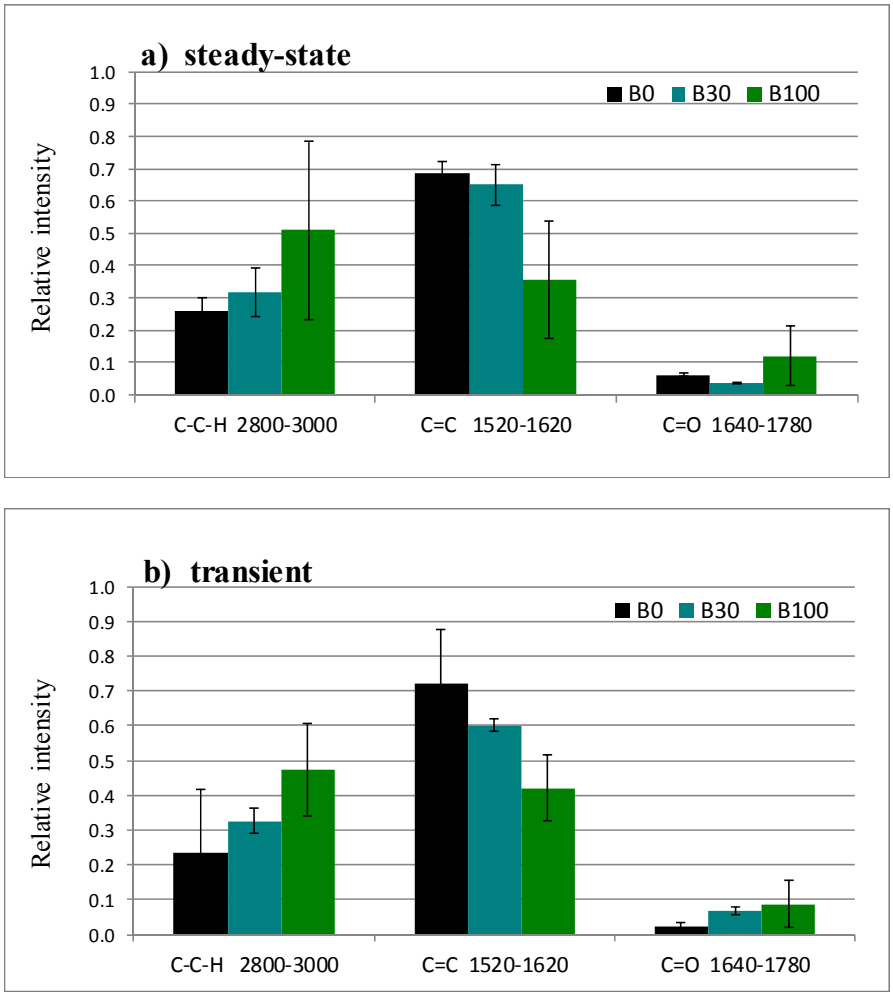

Fig. 3. Relative intensities of prominent bands of FTIR absorbance spectra relative to C-C-H, aromatic C=C, and O-containing groups in a) steady-state and b) transient conditions, using diesel (B0), 30% biodiesel (B30), and 100% biodiesel (B100). The spectral range of each functional group is indicated in cm^{-1}.

aliphatic C-C-H groups increases from around 22% for B0, up to 50% for B100 (Fig. 3(b)).

The slightly pronounced band at 1724 cm^{-1} of both carboxylic and carbonyl groups in diesel particles is changed to a band of C=O groups widen up to 1770 cm^{-1} with a shoulder at 1760 cm^{-1} in 30% biodiesel particles. Conversely, this band appears no longer as a shoulder but well separated and centered at 1770 cm^{-1} in 100% biodiesel particles. Since unsaturated alkenyl AlC=C bands were not emphasized in FTIR spectra of modern engine emission in transient conditions, but carbonyl functionalities were observed (Popovicheva *et al.*, 2015a), we assign the band at 1667 cm^{-1} to the stretching of carbonyls in quinines and conjugated ketones. The relative intensity of oxygenated groups is estimated to be 2% for B0 and increases up to 10% for B100 (Fig. 3(b)).

The second prominent FTIR feature of the spectra is represented by C=C vibrations in the 1570–1620 cm^{-1} region, similar to that observed for the steady-state condition, and relates to the polyaromatic character of diesel/biodiesel particle composition, although RC(O)O vibrations can broaden this band on the high frequency side. The relative intensity of aromatic C=C groups is estimated to be 70% for B0 and decreased to 40% for B100.

The major difference in the spectral features of 100% biodiesel particles emitted in transient condition is a broad band in the 3455–3650 cm^{-1} spectral range. It is assigned to hydroxyl stretching in alcohols and phenols, commonly observed in the combustion of oxygenated biofuel. A band near 2680 cm^{-1} indicates vibrations of a strong hydrogen bond in OH groups of carboxylic acids, strongly suggesting the formation of carboxylic acids in transient condition. A pronounced shoulder of the broad hydroxyl band at 3470 cm^{-1} is related to aromatic amino N-H stretches.

There is also a difference in composition between diesel and biodiesel particles in the 1533–1517 cm^{-1} region. This is associated to aromatic Ar-NO_2 vibrations in nitro compounds, while the features of aliphatic Al-NO_2 are absent in transient condition. For 100% biodiesel, the band of Ar-NO_2 groups at 1520 cm^{-1} is well resolved but for diesel and 30% biodiesel it is slightly visible as a shoulder of the broad band at 1580 cm^{-1}. Such spectral behavior indicates the more pronounced formation of nitro compounds when adding biodiesel to diesel.

Particle Composition by Mass Spectrometry

L2MS Analyses

Typical mass spectra recorded by L2MS with single-photon ionization (SPI) at 118 nm, and with R2PI at 266 nm for 100% biodiesel particles in steady-state condition are plotted in Fig. 4. Spectra corresponding to particulate emissions in the different working regimes are provided in Fig. S1 (Supplementary material). With 118 nm ionization, the most intense peaks (*m/z* 15, 29, 43, 57, 71, and 85) relate to alkyl fragments with $C_nH_{2n+1}^+$ series corresponding to normal and branched alkanes. They are accompanied by peaks of $C_nH_{2n-1}^+$ (*m/z* 69, 83, 97, 111, and 125) and $C_nH_{2n-3}^+$ formulas (*m/z* 67, 81, 95, and 109), which fragments are indicative of mono- and bi-cycloalkanes with alkyl side-chains, respectively (McLafferty and Turecek, 1993; Dallmann *et al*., 2014). In various studies (Tobias *et al*., 2001; Sakurai *et al*., 2003; Canagaratna *et al*., 2004), the predominance of *m/z* 69 over 71 and *m/z* 83 over 85 indicated a larger amount of cycloalkanes compared to alkanes, which was attributed to a larger relative contribution of lubricating oil compared to unburned fuel in the exhaust particles. In our case, *m/z* 71 and 85 always dominate this mass region, which suggests a relatively low oil impact on the organic content of the analyzed particles.

Peaks at *m/z* 74 and *m/z* 87 are only detected in spectra of biodiesel particles. *m/z* 74 is a characteristic fragment ($C_3H_6O_2^+$), which could be formed due to a McLafferty rearrangement reaction in methyl esters, while the *m/z* 87 ($C_4H_7O_2^+$) fragment corresponds to β-cleavage (Takayama *et al.*, 1995). The observation of both fragments emphasizes that all fatty acid methyl esters (FAME) in the biofuel were not fully burnt in the engine.

With ionization at 266 nm, the spectra of both diesel and biodiesel particles display mass peak distributions associated with PAHs and their alkylated derivatives (Figs. 4 and S2). The predominant peaks correspond to alkyl-anthracene/phenanthrene (*m/z* 178, 192, 206, 220, 234, 248, etc.) and alkyl-pyrene/fluoranthene (*m/z* 202, 216, 230, 244, 258, etc.) series. All mass peaks attributed to alkyl-PAH species exhibited some fragmentation of the side-chain, in ionization conditions for which no fragmentation of PAHs is observed. This point is strengthened by the observation of alkyl fragments in the low mass range *m/z* 0–100 (Fig. S3), as well as by the presence of *m/z* 91 associated with the tropylium cation ($C_7H_7^+$), which is the specific ion for the fragmentation of alkylbenzenes. The mass peak at *m/z* 94 related to the phenol ($C_6H_6O^+$) fragment shows that oxygenated aromatic compounds are present in the exhaust for all working regimes.

Discrimination between Operation Conditions by L2MS

Mass distributions vary only slightly with the fuel. However, some differences appear when considering different operating conditions. In Fig. S1, where mass spectra are obtained via the 118 nm ionization scheme, the spectra corresponding to the steady-state condition are characterized by a higher contribution of *m/z* 15 and 29 peaks compared to the transient condition. Another difference arises from the stronger intensity of *m/z* 42 and 56 peaks for the steady-state operating condition. These features are associated to the rearrangement of fragment ions from alkenes after the ionization process, as observed by Van Bramer and Johnston (1990) and Shi and Lipson (2005).

Fig. 5 represents the biplot of scores and loadings obtained by PCA for SPI L2MS data. The left and bottom axes are score scales (samples), while the right and upper

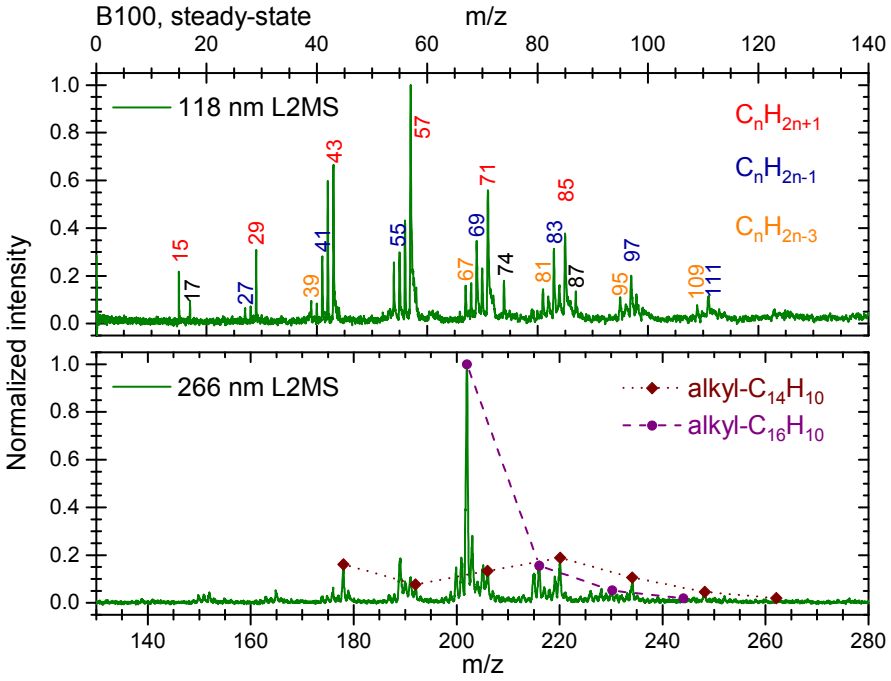

Fig. 4. L2MS spectra obtained with SPI at 118 nm (top panel) and R2PI at 266 nm (bottom panel) for particles emitted in steady-state conditions, using 100 % biodiesel (DB100S).

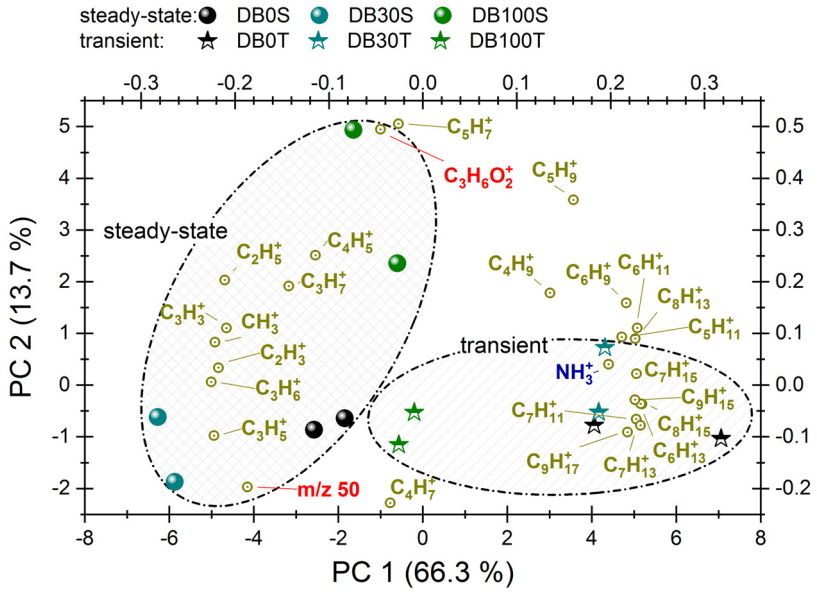

Fig. 5. Scores and loading biplot obtained for the first and second principal components representing 118 nm L2MS spectra of 2 blank zones and 12 zones analyzed on 6 different samples, as well as the 26 chemical components taken into account to perform the PCA (see text for details).

axes represent loadings (molecules) scales. The first principal component PC1 is composed by large hydrocarbon fragments (C_nH_m, $n \geq 4$) with positive coefficients and smaller fragments (C_nH_m, $n \leq 4$) with negative coefficients. Projection of samples onto PC1 brings out two clusters of points, discriminating to the two operating conditions. Particles produced in steady-state condition contain a larger amount of short chain fragments compared to particles from the transient cycle, which are characterized by longer chains. This property is in agreement with the observation of alkane fragment distribution shifted to lower masses in steady-state condition. None of the higher order principal components allowed a clear discrimination between the fuels. The aliphatic content in diesel/biodiesel particles depends more on the operating conditions than on the fuel. This can shed some light on the open question as to whether species detected in diesel/surrogates combustion emissions are of petrogenic or pyrogenic nature (Lemaire *et al.*, 2009). Further analysis of mass distributions in Fig. S1 shows that *m/z* 17 peak attributed to NH_3^+ is particularly prominent in transient operating condition for all fuels.

In R2PI L2MS spectra the difference between fuels is more noticeable. Spectra of biodiesel particles exhibit lower intensities of alkylated PAHs compared to PAHs, for both steady-state and transient conditions. The I_{206}/I_{178} peak intensity ratio between *m/z* 178 and 206 (representative masses for anthracene/phenanthrene and their C2-alkylderivatives) can be taken as an indicator of such a trend. Table 2 shows the decrease of the I_{206}/I_{178} ratio with the addition of biodiesel to diesel. The same trend appeared when calculating the $\sum I_{alkyl\text{-}PAHs}/\sum I_{total\ PAHs}$ ratio between the integrated peak area associated to alkyl-PAHs only and the integrated peak area due to all PAHs. We determined a 17.3% drop of the relative alkyl-PAH ion signal when passing from diesel to biodiesel in steady-state, and a 12.2% decrease in transient condition. Comparison of alkyl-anthracene/phenanthrene and alkyl-pyrene/fluoranthene mass distributions (Fig. S2 and Table 2) shows that the average number of sp^3 carbon in each alkyl-PAH series in slightly higher for steady-state compared to transient condition. This implies either larger aliphatic branches or the presence of more substitutive chains attached to PAHs.

The apparent discrepancy between spectra recorded with SPI at 118 nm and R2PI at 266 nm lies in the near absence of PAHs in 118 nm spectra, although VUV photons have enough energy to ionize them. This could result from the

Table 2. Alkyl-PAH distribution obtained by R2PI at 266 nm, alkyl-PAHs to PAHs integrated peak area ratio, the *m/z* 206 (C2-phenanthrene) to 178 (phenanthrene) integrated peak area ratio, and average carbon atom number *n* in C_n-phenanthrene and C_n-pyrene, reflecting the length and number of side-chains in alkyl-PAHs.

Operation condition	Fuel	$\sum I_{alkyl\text{-}PAHs}/\sum I_{total\ PAHs}$ (%)	I_{206}/I_{178}	n_{avg} in C_n-$C_{14}H_{10}$	n_{avg} in C_n-$C_{16}H_{10}$
steady-state	B0	63.7	3.56	2.57	0.80
	B30	64.2	3.14	2.81	0.93
	B100	46.4	1.22	2.40	0.37
transient	B0	58.1	3.77	2.08	0.49
	B30	56.2	2.95	2.19	0.54
	B100	45.9	1.32	2.22	0.41

much lower concentration of aromatic compared to aliphatic compounds in diesel/biodiesel emissions. Gentner *et al.* (2012) obtained similar chemical classes of dominant mass fragments in fuel and traffic-emitted aerosol composition and showed that carbon in total aliphatic compounds may make up to 68% by weight compared to 4% for polycyclic aromatic compounds.

SIMS Analyses

SIMS spectra for both positive and negative polarities are shown in Fig. 6(a) for 100% biodiesel particles produced in steady-state condition and in Figs. S4 and S5 for all fuels and conditions. Positive spectra are dominated by hydrocarbon $C_nH_m^+$ fragments and sodium Na^+. Masses between *m/z* 150 and 300 can be mostly attributed to PAHs. Signals assigned to K^+, Mg^+, Cu^+, and Zn^+ metallic ions are present in the mass spectra, and are more visible in the transient condition. Additional minor signals corresponding to NH_4^+ and oxygenated species, such as CH_3O^+ (*m/z* 31), $C_2H_5O^+$ (*m/z* 45), $C_2H_3O_2^+$ (*m/z* 59), and $C_3H_7O^+$ (*m/z* 59), are identified in the spectra. CH_3O^+ and $C_2H_5O^+$ fragments are proposed to be linked to methyl esters, ethers, primary

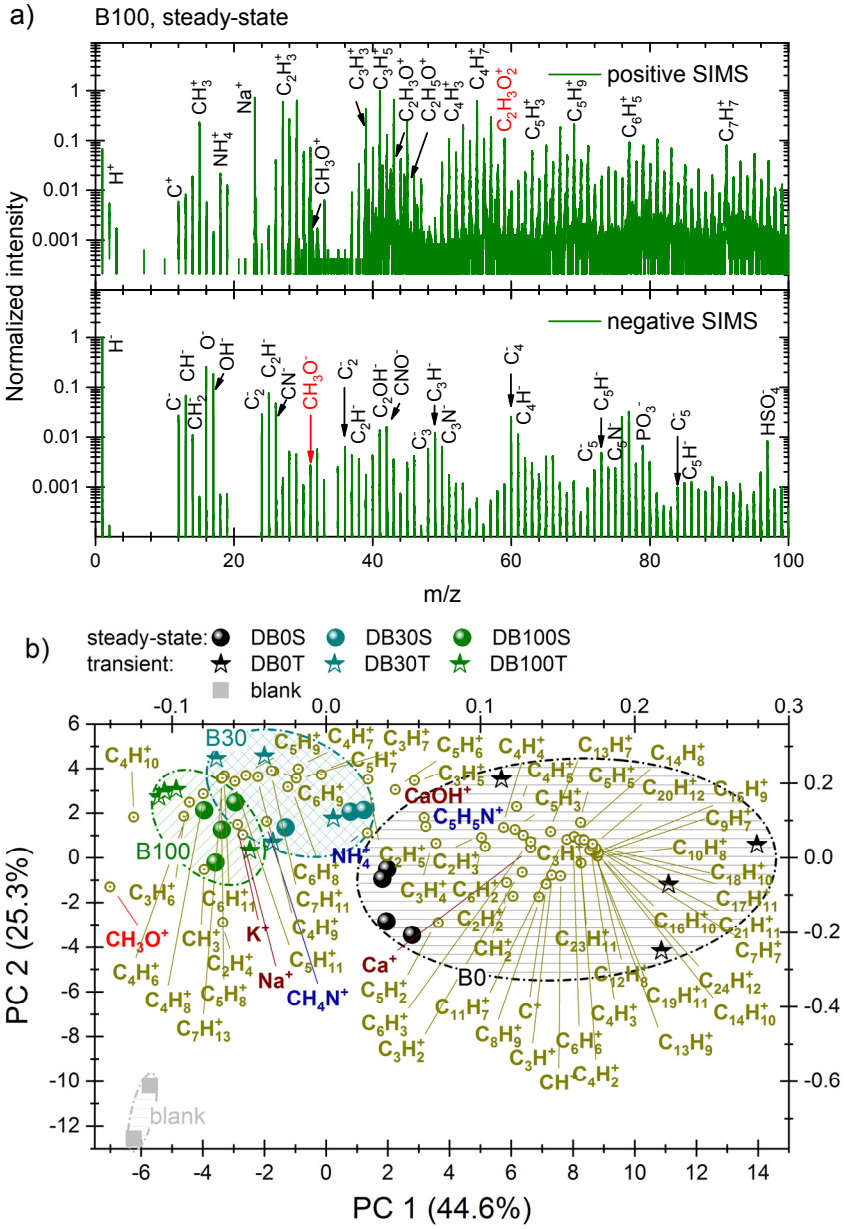

Fig. 6. a) Positive and negative SIMS spectra of 100 % biodiesel particles emitted in steady-state condition. The main assigned fragment ions are displayed and biodiesel specific fragment ions at *m/z* 59 ($C_2H_3O_2^+$) and *m/z* -31 (CH_3O^-) are highlighted in red. b) Biplot obtained for the first and second principal components showing SIMS positive spectra of 2 blank zones and 23 zones analyzed on 6 different samples, along with the 67 chemical components considered to perform the PCA. c) Biplot obtained for the first and second principal components showing SIMS negative spectra of 2 blank zones and 20 zones analyzed on 6 different samples, along with the 33 chemical components considered to perform the PCA.

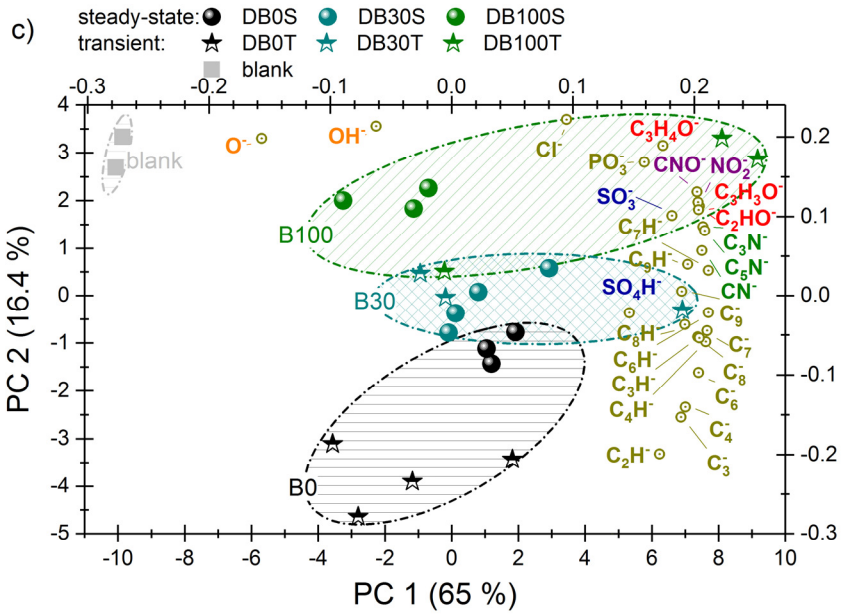

Fig. 6. (*continued*).

alcohols, and methyl carbinols (Scheinmann, 2013). The CH_3O^+ fragment (*m/z* 31) has also been associated to the fragmentation of methyl ester (Chien *et al.*, 2009). An increased relative concentration of this fragment is found in spectra of biodiesel particles compared to diesel ones (Fig. 7). Ion $C_3H_7O^+$ can arise from the fragmentation of dimethyl carbinols, while $C_2H_3O_2^+$ is associated to methyl esters, acetates, and acids (Scheinmann, 2013).

The *m/z* 59 mass peaks have been used to differentiate biodiesel *vs* diesel in high resolution ToF-AMS spectra (Choi *et al.*, 2015). Diesel particles were characterized by the $C_3H_7O^+$ component (*m/z* 59.04) only, whereas biodiesel particles were dominated by the $C_2H_3O_2^+$ fragment (*m/z* 59.01). We found the same trend in our spectra, as outlined by the red arrows in Fig. S4. The $C_2H_3O_2^+$ ion likely originates from the fragmentation of unburned methyl esters from biodiesel. Among oxygenated positive ions, *m/z* 59 and CH_3O^+ present a high correlation between their integrated peak areas normalized with respect to the total ion count (TIC). This means that these two fragments have the same source or they come from the same molecule. This correlation strengthens the common attribution of CH_3O^+ and $C_2H_3O_2^+$ to methyl esters.

Negative SIMS spectra are dominated by H^-, O^-, and OH^- fragment ions (Fig. 6(a)). Additional strong features correspond to the C_n^- and C_nH^- (n = 1–9) series with the hydrogenated carbon cluster C_nH^- being more intense compared to C_n^- when n is an even number (except in the case of n = 1). Such C_n^- carbon cluster series were observed by laser ablation particle mass spectrometry in petroleum fuel, biodiesel diffusion flames (Maricq *et al.*, 2011), and in spark generated soot (Kirchner *et al.*, 2003). C_n^- (n = 2–4) fragments were considered to be a marker for elemental carbon (EC) in aerosol mass spectrometry (AMS) data (Pagels *et al.*, 2013). This fact is confirmed by the high positive correlation factors between C_2^-, C_3^-, and C_4^-. The correlation between C_3^- and C_4^- is the highest (R^2 = 0.98), while the lowest positive correlation is between C_2^- and C_4^- (R^2 = 0.66).

Main fragments in negative ion spectra associated to nitrogenized species are NO_x reaction products CN^- (*m/z* -26), C_3N^- (*m/z* -50), C_5N^- (*m/z* -74), CNO^- (*m/z* -28) and NO_2^- (*m/z* -46) (Figs. 6(a) and S3). The main identified oxygenated fragments are CH_3O^- (*m/z* -31), C_2HO^- (*m/z* -41), $C_3H_3O^-$ (*m/z* -55), $C_3H_4O^-$ (*m/z* -56), and $C_2H_3O_2^-$ (*m/z* -59). The $C_2H_3O_2^-$ acetate fragment ion was proposed in AMS studies as a marker for oxidized organics from pyrolysis of cellulose (Silva *et al.*, 1999; Pagels *et al.*, 2013). In our study $C_2H_3O_2^-$ relative intensity increases from B0 to B100 for both regimes with a higher contrast for the transient cycle (Fig. 7). CH_3O^- (*m/z* -31) can be considered as a characteristic fragment for biodiesel, as it is almost absent in diesel particles and shows up in much higher abundance on biodiesel ones.

The normalized intensities of specific fragments (Na^+, CH_3O^+, CNO^-, CH_3O^-, C_2HO^-, $C_3H_3O^-$, $C_2H_3O_2^-$, CN^-, C_3N^-, NO_2^-, PO_3^-, SO_3^-, and Cl^-) and fragment families (PAH^+ and C_n^-) are plotted in Fig. 7 with error bars corresponding to the standard deviation associated with the multiple zones analyzed on each sample. The normalized signals obtained for the blank filter are given for comparison. For most of the fragments, the blank filter relative intensities are negligible compared to the sample relative signals. For the remaining fragments, comparison with the blank depends on ion polarity. In positive polarity, the total ion count (TIC) for the samples is at least one order of magnitude higher than for the blank. This means that the CH_3O^+ intensity is at least ten times higher in the samples compared to the blank. In negative polarity, TICs are similar for the samples and the blank.

The relative proportion of C_n^- fragments decreases from diesel to biodiesel particles. This result is in good agreement

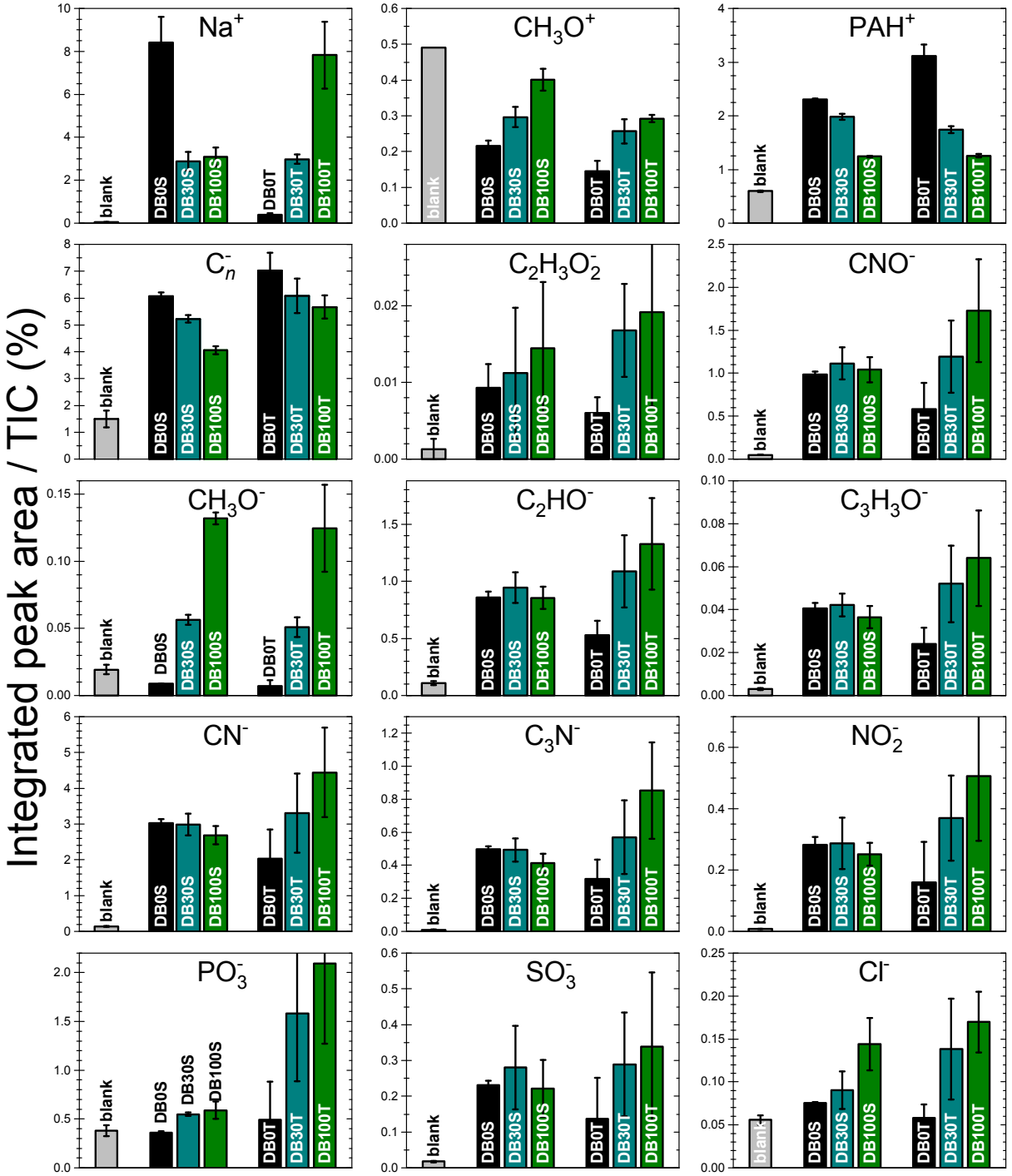

Fig. 7. Integrated peak areas of positive and negative SIMS fragment ions normalized to total ion count (TIC) for the different regimes. The error bars are calculated as the standard deviation obtained for the number of zones analyzed on each sample.

with EC measurements (Fig. 1(a)). Apart from specific fragments CH_3O^+, PAH^+, C_n^-, and CH_3O^-, the relative abundances of nitrogenized and other oxygenated fragments remain almost unchanged in steady-state condition, whereas in transient cycle some of these fragments increase with the addition of biodiesel.

Sodium (Na^+), chlorine (Cl^-), phosphates (PO_3^-), and sulfur oxide (SO_3^- and SO_4^-) complete the inorganic composition of diesel/biodiesel particles (Fig. 7). Na^+ has a significant contribution in the mass spectra corresponding to B0 in steady-state condition, while remaining constant for B30 and B100. On the contrary, transient condition shows an increase of the Na^+ component from B0 to B100. The absence of a clear correlation with fuel composition is also observed for bulk ion masses (Fig. 1(b)). It is probably due to the fact that the concentration of mineral impurities is

significantly higher in lubrication oil than in the fuel.

A positive correlation factor is found between Na^+ and K^+, indicating that these two elements have the same source. K^+ relative intensity increases linearly from B0 to B100 at transient condition, while for steady state its values are almost constant. The same trend is observed from ions measurements (Fig. 1(b)). Furthermore, Mg^+ ion has a positive correlation with Ca^+ ($R^2 = 0.76$) and Zn^+ ($R^2 = 0.72$). These elements are discernable for the transient condition, while for the steady state one their signals are comparable to the blank. In this case, their relative intensities are higher in B0 and display a 3-fold decrease for B30.

Discrimination between Working Regimes by SIMS

PCA has been applied to selected peaks from SIMS spectra, as explained above. Scatter plots for the first two components PC1 and PC2 are displayed in Fig. 6. For the positive ions, PC1 (44.6% variance) provides the best separation between the working regimes. For B0 in both operation conditions, the positive loadings of selected PAHs ($C_nH_m^+$ with $n \geq 10$) and low-hydrogenated hydrocarbons ($C_nH_m^+$ with $m \leq n$) are emphasized. B100 and B30 are separated from B0 through the negative loadings of PC1, which correspond to hydrogen-rich carbon fragments, Na^+, K^+, and oxygenated fragments. Hydrogen-rich carbon fragments are associated to aliphatic compounds. The samples are more discriminated by the nature of the fuel than by the engine operating conditions. Diesel particles emitted in transient condition have a richer PAH content due to higher positive scores obtained for PC1 (Fig. 6(b)). The differentiation between the operating conditions decreases for B30 and is almost indiscernible for B100.

For the negative ions, PC1 (65% variance) separates the regimes containing C_n^- and C_nH^- fragments from those showing larger amounts of O^-, OH^-, and SiO_2^-, which are corresponding to blanks (Fig. 6(c)). PC2 discriminates between the C_n^- and C_nH^- carbon fragments having negative coefficients and the other oxygenated, nitrogenated and sulfur containing fragments with positive coefficients. With positive scores on PC2, biodiesel particles are richer in nitrogenated and oxygenated compounds. As in the case of PCA for positive ions, the highest discrimination is observed with respect to the fuels. Conversely, B100 particles are separated by the operating conditions. These statistical analyses show that the most abundant compounds are not significantly different between all working regimes, as the loadings do not exceed 0.3. However, they allowed a clear separation on the fuel, biodiesel particles being characterized as more oxidized and nitrogenized, and having a higher aliphatic to PAH ratio compared to diesel particles.

DISCUSSION

Different classes of C_1 through C_{30} organic compounds, such as alkanes, PAHs, alkyl-PAHs, n-alkanoic and alkanedioic acids, are identified in diesel/biodiesel particulate exhaust (Schauer *et al.*, 1999; Casal *et al.*, 2014). The origin of alkanes and cycloalkanes in diesel emission is mainly attributed to unburned fuel and/or lubricating oil (Tobias *et al.*, 2001; Sakurai *et al.*, 2003; Dallmann *et al.*, 2014). Aliphatic groups are commonly observed in emissions of off-road diesel engines (Kirchner *et al.*, 2003; Popovicheva *et al.*, 2014, 2015b), as well as in modern internal combustion engines (Popovicheva *et al.*, 2015a) operating in various cycles and at different loads.

In our study, the predominant FTIR spectral features in diesel and biodiesel particles emitted by a heavy-duty diesel engine operated in steady-state condition are the aromatic C=C bands, which can be attributed to both polyaromatic compounds and soot microcrystalline structure. The aromatic ring stretching band at near 1600 cm^{-1} along with the absence of the aromatic C-H stretching band at 3040 cm^{-1} suggest a higher contribution from the low-hydrogenated and compact polyaromatic structure of the soot microstructure instead of polycyclic aromatic hydrocarbons.

Formation of saturated aliphatic C-C-H bands originating in alkanes accompanies soot formation. Their relative intensities indicate the increase of alkane species and the decrease of polyaromatic compounds when adding biofuel to diesel. A similar trend is inferred from the most intense peaks corresponding to alkyl fragments with $C_nH_{2n+1}^+$ series related to normal and branched alkanes, accompanied by mono- and bi-cycloalkanes with alkyl side-chains, and to PAHs and their alkylated derivatives, preferably indicating the contribution of unburned fuel compared to lubricating oil. A much lower contribution of aromatics compared to that of aliphatic compounds is observed for biodiesel emissions. The predominant aromatic peaks are alkyl-anthracene/phenanthrene and alkyl-pyrene/fluoranthene series for both regimes.

FTIR results indicate that the carbonyl C=O band in anhydrides and esters become prominent in biodiesel particles. Similarly, MS indicates that the two $C_3H_6O_2^+$ and $C_4H_7O_2^+$ fragments follow the same trend, and are thus unambiguously attributed to methyl esters fragments, along with the CH_3O^+, $C_2H_5O^+$, and $C_2H_3O_2^+$ ions. Because C=C and carboxylate RC(O)O vibrations overlap, the interpretation of the band near 1600 cm^{-1} is difficult. However, MS results indicate an increase of the $C_2H_3O_2^-$ acetate ion relative intensity with the addition of biodiesel to diesel. This observation is supported by the presence of $RCOO^-$ ions in carboxylic acids and salts, as confirmed by the positive correlation values of $C_2H_3O_2^-$ with Na^+ ($R^2 = 0.20$), K^+ ($R^2 = 0.55$), and NO_2^- ($R^2 = 0.78$).

The pattern of functionalities determined by aromatic, aliphatic, carboxylic, and carbonyls is a characteristic for diesel/biodiesel particles in transient condition, with the similar tendency when adding biofuel into diesel. The mass peak distribution of alkyl fragments is shifted to lower values for particles produced in steady-state condition. This behavior is in agreement with the observation of the symmetric/asymmetric stretches and bends of methylene > CH_2 groups in alkanes, which follows the same trend as that observed for MS fragments. The major difference in the spectral features of 100% biodiesel particles in transient condition is the bands assigned to hydroxyl OH stretching in alcohols, phenols and carboxylic acids, produced by combustion of oxygenated biofuel. The relative amounts of

PAH^+ and C_n^- fragments slightly increase in transient condition. Functionalities of aliphatic and aromatic $-NO_2$ in nitro compounds become prominent when changing diesel to biodiesel in both operating conditions. They appear as nitrogenized CN^-, C_3N^-, C_5N^-, CNO^-, and NO_2^- fragments.

Fly ash in exhaust contains mostly transition and alkali earth metals and water-soluble ions produced by inorganic contaminations in lubricating oil and engine wear (Oanh *et al.*, 2010; Popovicheva *et al.*, 2014a; Shah *et al.*, 2014). Therefore, we observe no correlations with fuel for Na^+, K^+, Ca^{2+}, Cl^-, and PO_4^{3-} ions. Ammonium $NH4^+$ ions should be also noted because their spectral features are observed in 100% biodiesel particles in steady-state condition. Sulfates SO_4^{2-} and SO_3^-, which are commonly assigned to pollution of diesel emission (Popovicheva *et al.*, 2014a, b), are observed at relatively small concentrations due to low sulfate abundance in the conventional diesel fuel EN 590 used.

A fuel is considered to be good when its use leads to low PM emissions at both low and high engine speeds, and conversely is not recommended if it emits low PM at low engine speeds and high PM at high engine speeds (Agarwal *et al.*, 2011). This conclusion was extended also to chemical components in Xue *et al.* (2010). Our PCA study is a strong point confirming that B100 suffers a "more complete" combustion process, regardless of the engine operating conditions. The first component PC1 mainly differentiate the emitted particles by the nature of the fuel that was processed in the engine; the fuel blend B30 ranks in an intermediate position between diesel B0 and biodiesel B100. Diesel particles with positive PC1 scores are characterized by a higher PAH content, whereas a larger aliphatic fraction better represents biodiesel soot, which may be again a consequence of the fuel content (EPA report, 2002; Zhu *et al.*, 2016). The second component PC2 accounting for a lower variance does not allow a better discrimination between the PM samples, but gives a clear separation of the blanks, as shown in Fig. 6(c). Negative PC2 values for the blanks are mainly associated with very small hydrocarbons (C^+, CH^+, CH_2^+, and $C_2H_4^+$).

CONCLUSIONS

This work extends previous studies to a more complex chemical characterization of diesel and biodiesel emissions released in typical engine operating conditions. FTIR, L2MS, and SIMS spectrometry yield a more complete picture of particle functionalities, individual compounds, fragments, and ions, and hence expand our understanding of the complex organic chemical composition making up PM emitted in the environment by alternative fuel combustion.

The composition of particles produced by biodiesel in comparison with conventional diesel shows an increased abundance of classes of polar oxygenates and nitro compounds containing carbonyl and hydroxyl functional groups, as well as nitro groups. Our findings highlight *functional markers* of the organic structure, allowing for a better evaluation of the relationship between engine, fuel, engine operating condition and particle composition, thus improving the quantification of environmental impacts of alternative energy source emissions.

L2MS using single photon ionization (SPI) and resonant two-photon ionization (R2PI), and positive and negative SIMS complete the identification of individual compounds by the detection of molecular species and specific fragments. The use of biodiesel instead of diesel results in the production of additional molecular species directly linked to the ester character of biodiesel, but also lessens the PAH and EC content. In contrast, the change from steady-state to transient conditions modifies species distribution inside the various classes of compounds. The lowest variance on chemical compounds is observed by PCA for diesel, while the addition of biodiesel to diesel leads to a higher separation by the engine operating condition. By combining PCA results obtained with positive and negative SIMS we can conclude that the best approach for a "controlled" (i.e., independent of the operating conditions) particle chemical composition is to use the combined biodiesel/diesel blend. The general agreement between chemical bonds and molecular/ions fragments identified by FTIR spectroscopy and mass spectrometry indicates the complementary character of both techniques and remove uncertainties concerning the interpretations of classes of organic compounds. In addition, it improves the identification of classes of organic and inorganic compounds in oxygenated biodiesel that differs from that observed for diesel emission, and distinguishes the various engine operating conditions at the molecular level of particulate characterization.

These results demonstrate the potential impact of biodiesel blending on the chemical characteristics of diesel emissions. The importance of health-related properties assigned to functionalized structure and molecular species of engine-produced particles indicates that their composition may be significantly changed upon transition from diesel to alternative fuels. The knowledge of chemical reactive forms of carbonaceous emissions can contribute to the planning of air quality control strategies and help the interpretation of the transport-emitted particle interactions with the environment.

ACKNOWLEDGMENTS

Financial support from Czech Science Foundation BIOTOX (13-0148S) and RFBR–VAST 15-55-54020 project is acknowledged. This work was partially supported by the Agence Nationale de la Recherche through the LABEX CAPPA (ANR-11-LABX-0005), as well as by the Ministry of Higher Education and Research, Hauts de France Regional Council and European Regional Development Fund (ERDF) through the Contrat de Projets Etat-Region (CPER CLIMIBIO). Support from the PEMs4Nano project funded by the European Union's Horizon2020 Programme for research, technological development and demonstration under Grant Agreement no. 724145 is also acknowledged.

SUPPLEMENTARY MATERIAL

Supplementary data associated with this article can be found in the online version at http://www.aaqr.org.

REFERENCES

Abdullah, M.F.E.B., Madzrol, N.B. and Sandin, R.W.A.P. (2016). Effects of biodiesel saturation degrees on NO_x emission and FTIR spectroscopy. *J. Appl. Sci. Process Eng.* 3: 24-33.

Agarwal, A.K. (2007). Biofuels (alcohols and biodiesel) applications as fuels for internal combustion engines. *Prog. Energy Combust. Sci.* 33: 233–271.

Agarwal, A.K., Gupta, T. and Kothari, N. (2011). Particulate emissions from biodiesel vs diesel fueled compression ignition engine. *Renewable Sustainable Energy Rev.* 15: 3278–3300.

Bauer, J.J., Yu, X.Y., Cary, R., Laulainen, N. and Berkowitz, C. (2009). Characterization of the Sunset semi-continuous carbon aerosol analyzer. *J. Air Waste Manage. Assoc.* 59: 826–833.

Bernstein, J.A., Alexis, N., Barnes, C., Bernstein, I.L., Bernstein, J.A., Nel, A., Peden, D., Diaz-Sanchez, D., Tarlo, S.M. and Williams, P.B. (2004). Health effects of air pollution. *J. Allergy Clin. Immunol.* 114: 1116–1123.

Betha, R. and Balasubramanian, R. (2011). Emissions of particulate-bound elements from stationary diesel engine: Characterization and risk assessment. *Atmos. Environ.* 45: 5273–5281.

Bladt, H., Schmid, J., Kireeva, E., Popovicheva, O.B., Perseantseva, N.M., Timofeev, M.A., Heister, K., Uihlein, J., Ivleva, N.P. and Niessner, R. (2012). Impact of Fe content in laboratory-produced soot aerosol on its composition, structure and thermo-chemical properties. *Aerosol Sci. Technol.* 46: 1337–1348.

Bouvier, Y., Mihesan, C., Ziskind, M., Therssen, E., Focsa, C., Pauwels, J.F. and Desgroux, P. (2007). Molecular species adsorbed on soot particles issued from low sooting methane and acetylene laminar flames: A laser-based experiment. *Proc. Combust. Inst.* 31: 841–849.

Butcher, D.J. (1999). Vacuum ultraviolet radiation for single-photoionization mass spectrometry: A review. *Microchem. J.* 62: 354–362.

Casal, C.S., Arbilla, G. and Corrêa, S.M. (2014). Alkyl polycyclic aromatic hydrocarbons emissions in diesel/biodiesel exhaust. *Atmos. Environ.* 96: 107–116.

Chang, Y.C., Lee, W.J., Yang, H.H., Wang, L.C., Lu, J.H., Tsai, Y.I., Cheng, M.T., Young, L.H. and Chiang, C.J. (2014). Reducing emissions of persistent organic pollutants from a diesel engine by fueling with water-containing butanol diesel blends. *Environ. Sci. Technol.* 48: 6010–6018.

Chen, Y., Shah, N., Braun, A., Huggins, F.E and Huffman, G.P. (2005). Electron microscopy investigation of carbonaceous particulate matter generated by combustion of fossil fuel. *Energy Fuels* 19: 1644–1651.

Chien, Y.C., Lu, M., Chai, M. and Boreo, F.J. (2009). Characterization of biodiesel and biodiesel particulate matter by TG, TG-MS, and FTIR. *Energy Fuels* 23: 202–206.

Choi, Y, Choi, J., Park, T., Kang, S. and Lee, T. (2015). Characterization of particulate emissions from biodiesel using high resolution time of flight aerosol mass spectrometer. *Asian J. Atmos. Environ.* 9: 75–85.

Chow, J.C., Yu, J.Z., Watson, J.G., Ho, S.S.H., Bohannan, T.L., Hays, M.D. and Fung, K.K. (2007). The application of thermal methods for determinating chemical composition of carbonaceous aerosols: A review. *J. Environ. Sci. Health* 42: 1521–1541.

Cofala, J., Amann, M., Klimont, Z., Kupiainen, K. and Hoeglung-Isaksson, H.L. (2007). Scenarios of global anthropogenic emissions of air pollutants and methane until 2030. *Atmos. Environ.* 41: 8486–8499.

Coury, C. and Dillner, A.M. (2009). ATR-FTIR characterization of organic functional groups and inorganic ions in ambient aerosols at a rural site. *Atmos. Environ.* 43: 940–948.

Dallmann, T.R., Onasch, T.B., Kirchstetter, T.W., Worton, D.R., Fortner, E.C., Herndon, S.C., Wood, E.C., Franklin, J.P., Worsnop, D.R., Goldstein, A.H. and Harley, R.A. (2014). Characterization of particle matter emission from on-road gasoline and diesel vehicles using soot particle aerosol mass spectrometer. *Atmos. Chem. Phys*. 14: 7585–7599.

Delhaye, D., Ouf, F.-X., Ferry, D., Ortega, I.K., Penanhoat, O., Peillon, S., Salm, F., Vancassel, X., Focsa, C., Irimiea, C., Harivel, N., Perez, B., Quinton, E. and Gaffié, D. (2017). MERMOSE project: characterization of particle emissions of a commercial aircraft engine. *J. Aerosol Sci.* 105: 48–63.

Desgroux, P., Mercier, X. and Thomson, K.A. (2013). Study of the formation of soot and its precursors in flames using optical diagnostics. *Proc. Combust. Inst.* 34: 1713–1738.

Dwivedi, D., Agarwal, A.K. and Sharma M. (2006). Particulate emission characterization of a diesel vs diesel-fueled compression ignition transport engine: a comparative study. *Atmos. Environ.* 40: 5586–5595.

EPA Report (2002). *A comprehensive analysis of biodiesel impacts on exhaust emissions*, U. S.EPA. EPA420-P-02-001.

Faccinetto, A., Desgroux, P., Ziskind, M., Therssen, E. and Focsa, C. (2011). High-sensitivity detection of polycyclic aromatic hydrocarbons adsorbed onto soot particles using laser desorption/laser ionization/time-of-flight mass spectrometry: An approach to studying the soot inception process in low pressure flames. *Combust. Flame* 158: 227–239.

Faccinetto, A., Focsa, C., Desgroux, P. and Ziskind, M. (2015). Progress toward the quantitative analysis of PAHs adsorbed on soot by laser desorption/laser ionization/time-of-flight mass spectrometry. *Environ. Sci. Technol.* 49: 10510–10520.

Ferge, T., Mühlberger, F. and Zimmermann, R. (2005). Application of infrared laser desorption vacuum-UV single photon ionization mass spectrometry for analysis of organic compounds from particulate matter filter samples. *Anal. Chem.* 47: 4528–4538.

Focsa, C. and Destombes, J.L. (2001). $Na/K(H_2O)_n$ clusters produced by laser desorption of Na/K salt doped ice. *Chem. Phys. Lett.* 347: 390–396.

Focsa, C., Chazallon, B. and Destombes, J.L. (2003). Resonant desorption of ice with a tunable $LiNbO_3$ optical parametric oscillator. *Surf. Sci.* 528: 189–195.

Geller, M.D., Ntziachristos, L., Mamakos, A., Samaras, Z., Schmitz, D.A., Froines, J.R. and Sioutas, C. (2006). Physicochemical and redox characteristics of particulate matter (PM) emitted from gasoline and diesel passenger cars. *Atmos. Environ.* 40: 6988–7004.

Gentner, D.R., Isaacman, G., Worton, D.R., Chan, A.W.H., Dallmann, T.R., Davis, L., Liu., S., Day, D.A., Russell, L.M., Wilson, K.R., Weber, R., Guha, A., Harley, R.A. and Goldstein, A. H. (2012). Elucidating secondary organic aerosol from diesel and gasoline vehicles through detailed characterization of organic carbon emissions. *Proc. Natl. Acad. Sci. U.S.A.* 109: 18318–18323.

Giakoumis, E.G., Rakopoulos, C.D., Dimaratos, A.M. and Rakopoulos, D.C. (2012). Exhaust emissions of diesel engines operating under transient conditions with biodiesel fuel blends. *Prog. Energy Combust. Sci.* 38: 691–715.

Guzman-Morales, J., Frossard, A.A., Corrigan, A.L., Russell, L.M., Liu, S., Takahama, S., Taylor, J.W., Allan, J., Coe, H., Zhao, Y. and Goldstein, A.H. (2014). Estimated contributions of primary and secondary organic aerosol from fossil fuel combustion during the CalNex and Cal-Mex campaigns. *Atmos. Environ*. 88: 330–340.

Jedynska, A., Tromp, P.C., Houtzager, M.M.G. and Kooter, I.M. (2015). Chemical characterization of biofuel exhaust emissions, *Atmos. Environ.* 116: 172–182.

Jung, H., Kittelson, D.B., Zachariah, M. (2006). Characteristics of SME biodiesel-fueled diesel particle emissions and the kinetics of oxidation. *Environ. Sci. Technol.* 40: 4949–4955.

Karavalakis, G., Bakeas, E., Fontaras, G. and Stournas, S. (2011). Effect of biodiesel origin on regulated and particle-bound PAH (polycyclic aromatic hydrocarbon) emissions from a Euro 4 passenger car. *Energy* 36: 5328–5337.

Karavalakis, G., Boutsika, V., Stournas, S. and Bakeas, E. (2011). Biodiesel emissions profile in modern diesel vehicles. Part 2: Effect of biodiesel origin on carbonyl, PAH, nitro-PAH and oxy-PAH emissions. *Sci. Total Environ.* 409: 738–747.

Kirchner, U., Vogt, R., Natzeck, C. and Goschnick, J. (2003). Single particle MS, SNMS, SIMS, XPS, and FTIR spectroscopic analysis of soot particles during the AIDA campaign. *J. Aerosol Sci.* 34: 1323–1346.

Kleeman, M., Schauer, J. and Cass, J. (2000). Size and composition distribution of fine particulate matter emitted from motor vehicles. *Environ. Sci. Technol.* 34: 1132–1142.

Lemaire, R., Faccinetto, A., Therssen, E., Ziskind, M., Focsa, C. and Desgroux, P. (2009). Experimental comparison of soot formation in turbulent flames of diesel and surrogate diesel fuels. *Proc. Combust. Inst.* 32: 737–744.

Libalova, H., Rossner, P., Vrbova, K., Brzicova, T., Sikorova, J., Vojtisek-Lom, M., Berenk, V., Klem, J., Ciganek, M., Neca, J., Pencikova, K., Machala, M. and Topinka, J. (2016). Comparative analysis of toxic response of organic extracts from diesel and selected alternative fuels engine emissions in human lung BEAS-2B cells. *Int. J. Mol. Sci.* 17: 1–24.

Lin, S.L., Tsai, J.H., Chen, S.J., Huang, K.L., Lin, C.C., Huang, H.T., Hsieh, Y.C. and Chiu. C.H. (2017). Emissions of polycyclic aromatic hydrocarbons and particle-bound metals from a diesel engine generator fueled with waste cooking oil-based biodiesel blends. *Aerosol Air Qual. Res.* 17: 1579–1589.

Maricq, M.M. (2011). Physical and chemical comparison of soot in hydrocarbon and biodiesel fuel diffusion flames: A study of model and commercial fuels. *Combust. Flame* 158: 105–116.

Mihesan, C., Lebrun, N., Ziskind, M., Chazallon, B., Focsa, C. and Destombes, J.L. (2004). IR laser resonant desorption of formaldehyde-H_2O ices: Hydrated cluster formation and velocity distribution. *Surf. Sci.* 566-568: 650–658.

Mihesan, C., Ziskind, M., Therssen, E., Desgroux, P. and Focsa, C. (2006). IR laser resonant desorption of polycyclic aromatic hydrocarbons. *Chem. Phys. Lett.* 423: 407–412.

Mihesan, C., Ziskind, M., Therssen, E., Desgroux, P. and Focsa, C. (2008). Parametric study of polycyclic aromatic hydrocarbon laser desorption. *J. Phys.: Condens. Matter* 20: 025221.

Moldanová, J., Fridell, E., Popovicheva, O., Demirdjian, B., Tishkova, V., Faccinetto, A. and Focsa, C. (2009). Characterization of particulate matter and gaseous emissions from a large ship diesel engine. *Atmos. Environ.* 43: 2632–2641.

Müller, J.-O., Su, D.S., Jentoft, R.E., Kröhnert, J., Jentoft, F.C. and Schlögl, R. (2005). Morphology-controlled reactivity of carbonaceous materials towards oxidation. *Catal. Today* 102-103: 259–265.

Na, K., Biswas, S., Robertson, W., Sahay, K., Okamoto, R., Mitchell, A. and Lemieux, S. (2015). Impact of biodiesel and renewable diesel on emissions of regulated pollutants and greenhouse gases on a 2000 heavy duty diesel truck. *Atmos. Environ.* 107: 307–314.

Oanh, N.T.K., Thiansathit, W., Bond, T.C., Subramanian, R., Winijkul, E. and Pawarmart, I. (2010). Compositional characterization of $PM_{2.5}$ emitted from in-use diesel vehicles. *Atmos. Environ.* 44: 15–22.

Pagels, J., Dutcher, D.D., Stolzenburg, M.R., McMurry, P.H., Gälli, M.E. and Gross, D.S. (2013) Fine-particle emissions from solid biofuel combustion studied with single-particle mass spectrometry: Identification of markers for organics, soot, and ash components. *J. Geophys. Res. Atmos.* 118: 859–870.

Pei, L., Jiang, G., Tyler, B.J., Baxter, L.L. and Linford, M.R. (2008). Time-of-flight ion mass spectrometry of a range of coal samples: A chemometrics (PCA, Cluster, and PLS) analysis. *Energy Fuels* 22: 1059–1072.

Popovicheva, O., Engling, G., Lin, K.T., Persiantseva, N., Timofeev, M., Kireeva, E., Volk, P., Hubert, A. and Wachtmeister, G. (2015a). Diesel/biofuel exhaust particles from modern internal combustion engines: Microstructure,

composition, and hygroscopicity. *Fuel* 157: 232–239.

Popovicheva, O., Kireeva, E., Shonija, N., Zubareva, N., Persiantseva, N., Tishkova, V., Demirdjian, J., Moldanova, J. and Smith, D.M. (2009). Ship particulate pollutants: Characterization in terms of environmental implication. *J. Environ. Monit.* 11: 2077–2086.

Popovicheva, O., Kistler, M., Kireeva, E., Persiantseva, N., Timofeev, M., Kopeikin, V. and Kasper-Giebl, A. (2014b). Physicochemical characterization of smoke aerosol during large-scale wildfires: Extreme event of August 2010 in Moscow. *Atmos. Environ.* 96: 405–414**.**

Popovicheva, O., Persiantseva, N.M., Shonija, N.K., DeMott P., Koehler, K., Petters, M., Kreidenweis, S., Tishkova, V., Demirdjian, B. and Suzanne, J. (2008). Water interaction with hydrophobic and hydrophilic soot particles. *Phys. Chem. Chem. Phys.* 10: 2332–2344.

Popovicheva, O.B., Engling, G., Diapouli, E., Saraga, D., Persiantseva, N.M., Timofeev, M.A., Kireeva, E.D., Shonia, N.K., Chen, S.H., Nguyen, D.L., Eleftheriadis, K. and Lee, C.T. (2016). Impact of smoke intensity on size-resolved aerosol composition and microstructure during the biomass burning season in Northwest Vietnam. *Aerosol Air Qual. Res.* 16: 2071–2654.

Popovicheva, O.B., Kireeva, E.D., Shonija, N.K., Vojtisek-Lom, M. and Schwarz J. (2015b). FTIR analysis of surface functionalities on particulate matter produced by off-road diesel engines operating on diesel and biofuel. *Environ. Sci. Pollut. Res. Int.* 22: 4534–4544.

Popovicheva, O.B., Kireeva, E.D., Steiner S., Rothen-Rutishauser, B., Persiantseva, N.M., Timofeev, M.A, Shonija, N.K, Comte P. and Czerwinski J. (2014a). Microstructure and chemical composition of diesel and biodiesel particle exhaust. *Aerosol Air Qual. Res.* 14: 1392–1401.

Popovicheva, O.B., Persiantseva, N.M., Kuznetsov, B.V., Rakhmanova, T.A., Shonija, N.K., Suzanne, J. and Ferry, D. (2003). Microstructure and water adsorbability of aircraft combustor soots and kerosene flame soots: Toward an aircraft-generated soot laboratory surrogate. *J. Phys. Chem. A* 107: 10046–10054.

Prokopowicz, A., Zaciera, M., Sobczak, A., Bielaczyc, P., Woodburn, J. (2015). The effects of neat biodiesel and biodiesel and HVO blends in diesel fuel on exhaust emissions from a light duty vehicle with a diesel engine. *Environ. Sci. Technol.* 49: 7473–7482.

Reff, A., Turpin, B.J., Offenberg, J.H., Weisel, C.P., Zhang, J., Morandi, M., Stock, T., Colome, S. and Winer, A. (2007). A functional group characterization of organic $PM_{2.5}$ exposure: Results from the RIOPA study. *Atmos. Environ.* 41: 4585–4598.

Russell, L.M., Bahadur, R., Hawkins, L.N., Allan, J., Baumgardner, D., Quinn, P.K. and Bates, T.S. (2009). Organic aerosol characterization by complementary measurements of chemical bonds and molecular fragments. *Atmos. Environ.* 43: 6100–6105.

Sakurai, H., Tobias, H.J., Park, K., Zarling, D., Docherty, K., Kittelson, D.B., McMurry, P.H. and Ziemann, P.J. (2003). On-line measurements of diesel nanoparticle composition and volatility. *Atmos. Environ.* 37): 1199–1210.

Schauer, J.J., Kleeman, M.J, Cass, G. and Simoneit, B. (1999). Measurement of emissions from air pollution sources. 2. C1 through C30 organic compounds from medium duty diesel trucks. *Environ. Sci. Technol.* 33: 1578–1587.

Scheinmann, F. (1973). *An Introduction to Spectroscopic Methods for the identification of organic compounds*, Pergamon Press, Oxford.

Shah, A.N., Yun-shan, G., Shah, F.H., Mughal, H.U., Rahman, Z.U. and Naveed, A. (2014). Effect of biodiesel on particulate numbers and composition emitted from turbocharged diesel engine. *Int. J. Environ. Sci. Technol.* 11: 385–394.

Shi, Y.J. and Lipson, R.H. (2005). An overview of organic molecule soft ionization using vacuum ultraviolet laser radiation. *Can. J. Chem*. 83: 1891–1902.

Singh, B.R. and Singh, O. (2012). In *Fossil Fuel and the Environment,* Khan, S. (Ed.), In Tech, p. 167.

Song, J., Alam, M., Boehman, A.L. and Kim. U. (2006). Examination of the oxidation behavior of biodiesel soot. *Combust. Flame* 146: 589–604.

Steiner, S., Czerwinski, J., Comte, P., Popovicheva, O.B, Kireeva, E., Müller, L., Heeb, N., Mayer, A., Fink, A. and Rothen-Rutishauser, B. (2013). Comparison of the toxicity of diesel exhaust produced by bio- and fossil diesel combustion in human lung cells in vitro. *Atmos. Environ.* 81: 380–388.

Tapia, A., Salgado M.S., Martín, P., Sanchez-Valdepeñas, J., Rossi, M.J. and Cabañas, B. (2015). The use of heterogeneous chemistry for the characterization of functional groups at the gas/particle interface of soot from a diesel engine at a particular running condition. *Environ. Sci. Pollut. Res. Int.* 22: 4863–4872.

Tapia, A., Salgado, M.S., Martín, M.P., Rodríguez-Fernández, J., Rossi, M.J. and Cabañas, B. (2017). Chemical characterization of diesel and hydrotreated vegetable oil (HVO) soot after reactive gas probing using diffuse reflectance FTIR spectroscopy (DRIFTS). *Environ. Sci. Pollut. Res. In*t. 24: 7534-7543.

Thomson, K., Ziskind, M., Mihesan, C., Therssen, E., Desgroux, P. and Focsa, C. (2007). Influence of the photoionization process on the fragmentation of laser desorbed polycyclic aromatic hydrocarbons. *Appl. Surf. Sci.* 253: 6435–6441.

Tobias, H.J., Beving, D.E., Ziemann, P.J., Sakurai, H., Zuk, M., McMurry, P.H., Zarling, D., Waytulonis, R., Kittelson, D.B. (2001). Chemical analysis of diesel engine nanoparticles using a nano-DMA/thermal desorption particle beam mass spectrometer. *Environ. Sci. Technol.* 35: 2233–2243.

Toner, S.M., Sodeman, D.A. and Prather, K.A. (2006). Single particle characterization of ultrafine and accumulation mode particles from heavy duty diesel vehicles using aerosol time-of-flight mass spectrometry. *Environ. Sci. Technol.* 40: 3912–3921.

Topinka, J., Milcova, A., Schmuczerova, J., Mazac, M., Pechout, M. and Vojtisek-Lom, M. (2012). Genotoxic potential of organic extracts from particle emissions of

diesel and rapeseed oil powered engines. *Toxicol. Lett*. 212: 11–17.

Turrio-Baldassarri, L., Battistelli, C.L., Conti, L., Crebelli, R., De Berardis, B., Iamiceli, A.L., Gambino, M. And Iannaccone, S. (2006). Evaluation of emission toxicity of urban bus engines: Compressed natural gas and comparison with liquid fuels. *Sci. Total Environ.* 355: 64–77.

Van Bramer, S.E. and Johnston, M.V. (1990). 10.5 eV Photoionization mass spectrometry of aliphatic compounds. *J. Am. Soc. Mass. Spectrom.* 1: 419–426.

Vander Wal, R.L., Yezerets, A., Currier, N.W., Kim, D.H. and Wang, C.M. (2007). HRTEM study of diesel soot collected from diesel particulate filters. *Carbon* 45: 70–77.

Vojtisek-Lom, M., Blažek, J., Dufek, M. and Fenkl, M. (2009). Investigation of combustion rates and injection and ignition onset of heated rapeseed oil in direct-injection turbodiesel engines. *SAE Technical Paper* 2009-01-1914.

Vojtisek-Lom, M., Czerwinski, J., Lenícek, J., Sekyra, M. and Topinka, J. (2012a). Polycyclic aromatic hydrocarbons (PAHs) in exhaust emissions from diesel engines powered by rapeseed oil methylester and heated non-esterified rapeseed oil. *Atmos. Environ.* 60: 253–261.

Vojtíšek-Lom, M., Pechout, M. and Barbolla, A. (2012b). Experimental investigation of the behavior of non-esterified rapeseed oil in a diesel engine mechanical fuel injection system. *Fuel* 97: 157–165.

Xue, J., Grift, T.E. and Hansen, A.C. (2011). Effect of biodiesel on engine performances and emissions. *Renewable Sustainable Energy Rev.* 15: 1098–1116.

Zhu, J., Wang, T., Talbot, R., Mao, H., Hall, C.B., Yang, X., Fu, C., Zhuang, B., Li, S., Han, Y. and Huang, X. (2012). Characteristics of atmospheric total gaseous mercury (TGM) observed in urban Nanjing, China. *Atmos. Chem. Phys*. 12: 12103–12118.

Zhu, L., Cheung, C.S. and Huang, Z. (2016). A comparison of particulate emission for rapeseed oil methyl ester, palm oil methyl ester and soybean oil methyl ester in perspective of their fatty ester composition. *Appl. Therm. Eng*. 94: 249–255.

Zoller, D.L., Sum, S.T., Johnston, V., Hatfield, G.R. and Qian, K. (1999). Determination of polymer type and comonomer content in polyethylenes by pyrolysis-photoionization mass Spectrometry. *Anal. Chem.* 71: 866–872.

Received for review, April 7, 2017
Revised, June 14, 2017
Accepted, June 15, 2017